NANO LETTERS

Letter

pubs.acs.org/NanoLett

# All-Color Plasmonic Nanolasers with Ultralow Thresholds: Autotuning Mechanism for Single-Mode Lasing

Yu-Jung Lu,[†] Chun-Yuan Wang,[†] Jisun Kim,[‡] Hung-Ying Chen,[†] Ming-Yen Lu,[∥] Yen-Chun Chen,[⊥] Wen-Hao Chang,[⊥] Lih-Juann Chen,[∥] Mark I. Stockman,[§,#,¶] Chih-Kang Shih,*[,‡] and Shangjr Gwo*[,†]

[†]Department of Physics, National Tsing-Hua University, Hsinchu 30013, Taiwan

[‡]Department of Physics, The University of Texas at Austin, Austin, Texas 78712, United States

[§]Center for Nanooptics (CeNO) and Department of Physics and Astronomy, Georgia State University, Atlanta, Georgia 30303, United States

[∥]Department of Materials Science and Engineering, National Tsing-Hua University, Hsinchu 30013, Taiwan

[⊥]Department of Electrophysics, National Chiao-Tung University, Hsinchu 30010, Taiwan

[#]Fakultät für Physik, Ludwig-Maximilians-Universität, Geschwister-Scholl-Platz 1, D-80539 München, Germany

[¶]Max-Planck-Institut für Quantenoptik, Hans-Kopfermann-Strasse 1, D-85748 Garching, Germany

*S* *Supporting Information*

**ABSTRACT:** We report on the first demonstration of broadband tunable, single-mode plasmonic nanolasers (spasers) emitting in the full visible spectrum. These nanolasers are based on a single metal−oxide−semiconductor nanostructure platform comprising of InGaN/GaN semiconductor nanorods supported on an $Al_2O_3$-capped epitaxial Ag film. In particular, all-color lasing in subdiffraction plasmonic resonators is achieved via a novel mechanism based on a property of weak size dependence inherent in spasers. Moreover, we have successfully reduced the continuous-wave (CW) lasing thresholds to ultrasmall values for all three primary colors and have clearly demonstrated the possibility of "thresholdless" lasing for the blue plasmonic nanolaser.

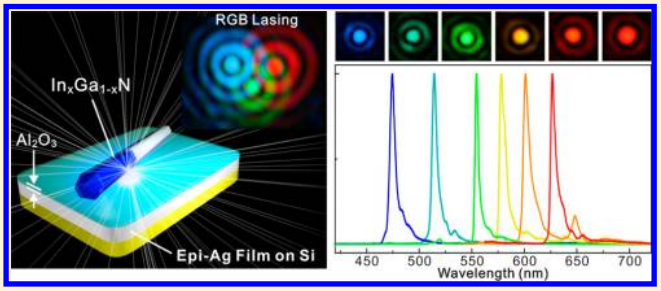


**KEYWORDS:** *Semiconductor nanolaser, plasmonic nanolaser, spaser, all-color lasing, thresholdless lasing, autotuning mechanism*

The realization of broadband-tunable semiconductor nanolasers with ultralow lasing thresholds can lead to transformative technological applications including all-optical, on-chip information processing, miniaturized smart display technology and hyperspectral, super-resolution biomedical imaging. However, conventional semiconductor lasers are limited in size, emission wavelength, and power consumption, resulting from the diffraction-limited minimum size of optical feedback resonators, inefficient semiconductor gain media in a broadly tunable emission range, and the requirement of lasing threshold. In the past two decades, tremendous research effort has been directed toward the development of novel semiconductor lasers such as microcavity lasers,[1] photonic crystal nanocavity lasers,[2−4] nanowire lasers,[5] and exciton-polariton lasers,[6] which allow for the long-sought-after subwavelength, thresholdless (ultralow threshold), and ultrafast laser operation. Moreover, a single-material semiconductor quantum dot system with tunable bandgap emissions has recently been applied to pursue all-color (red, green, blue; RGB) lasing.[7]

One promising approach to make such nanolasers possible is to utilize plasmonic resonators or cavities that support highly confined plasmon modes. Recent theoretical proposals[8−12] of surface plasmon amplification of stimulated emission of radiation (spaser) and experimental demonstrations[13−21] of plasmonic nanolasers have raised the prospects significantly. In contrast to the above-mentioned lasers,[1−7] which utilize optical feedback resonators to achieve lasing, the laser feedback mechanism of plasmonic nanolasers are based on the near-field coupling of gain media with adjacent metallic nanostructures that support highly confined surface plasmon modes. Recently, it has been demonstrated that plasmonic nanolasers can break the three-dimensional (3D) diffraction limit, making them, at present, the smallest lasers. However, until now, a clear demonstration of broadband tunability and ultralow threshold operation remains elusive for plasmonic nanolasers due to their intrinsic losses. In this work, we demonstrate that, by using a single metal−oxide−semiconductor (MOS) nanostructure platform with fully optimized material properties, single-mode plasmonic nanolasers tunable in the full visible spectrum can be realized with ultralow lasing thresholds. This remarkable

**Received:** April 6, 2014
**Revised:** July 5, 2014
**Published:** July 16, 2014

   dx.doi.org/10.1021/nl501273u | *Nano Lett.* 2014, 14, 4381−4388

phenomenon of broadband tunable, single-mode lasing without the need of precise cavity size control is understood through theoretical simulations that reveal a novel "auto tuning" mechanism consistent with properties of nanospasers whose generation frequency weakly depends on the resonator size.

The indium gallium nitride (InGaN) compound semiconductor alloy system has long been considered as a promising material for broadband tunable gain medium. The direct band gap of $In_xGa_{1-x}N$ ($0 \le x \le 1$) can be tuned from near-infrared (InN, 0.65 eV) to near-ultraviolet (GaN, 3.4 eV). Moreover, InGaN possesses a very large gain coefficient (on the order of $10^4$ $cm^{-1}$),[22] which is very beneficial for design of plasmonic lasers and amplifiers.[23,24] However, it has been recognized that for conventional wurtzite-structure InGaN/GaN heterostructures grown along the polar direction, the presence of strong polarization-induced interface charges would result in electron−hole separation in InGaN active regions, which can significantly reduce the radiative recombination efficiency.[25] This effect is particularly severe for InGaN/GaN heterostructures with a large indium content, as the increased strain further enhances the polarization field when emitting at longer wavelengths (e.g., green and red).[25−27] Several strategies have been developed to reduce this polarization effect and increase the luminescence efficiency of InGaN/GaN heterostructure.[25,27−29] Here, we adopt InGaN@GaN core−shell nanorod emitters with nonpolar side facets for this purpose.

The $In_xGa_{1-x}N$@GaN core−shell nanorods studied here were grown on Si(111) wafers by plasma-assisted molecular-beam epitaxy (PAMBE). The details of the growth procedure are given in the Supporting Information. Nanoscale structural and optical measurements of single nanorods confirm both the existence of nonpolar nanorod side facets (*m*-plane) and wide bandgap tunability. Scanning transmission electron microscopy (STEM) structural analysis of the InGaN@GaN nanorods reveal the InGaN core structure (9% indium content for the specific nanorod shows in Figure 1a). The lengths of nanorods measured for lasing characteristics range from 100 to 250 nm and their diameter is about 30 to 50 nm (see Supporting Information for details). It is important to note that these dimensions are too small to sustain lasing conditions using these nanorods alone as the photonic resonators.[5,30] Instead, lasing is realized by a plasmonic resonator structure based on a nanowire/nanorod MOS platform[31] comprising of a single InGaN@GaN nanorod supported on an $Al_2O_3$-capped epitaxial Ag film.

The photoluminescence (PL) spectra measured at room temperature show that PL from individual nanorods continuously spans the blue to red region of the visible spectrum (468−642 nm, see Figure 1b). The PL emission peaks are monochromatic and exhibit uniform intensity and line width, independent of In content, across the visible spectrum range. It should be emphasized that the greatly improved PL properties in the long-wavelength (high-In-content) regime is due to the absence of polar interfaces and surfaces. In the conventional wurtzite-type III-nitride heterostructures grown along the polar *c*-axis, the discontinuities of spontaneous and/or piezoelectric polarizations across the heterojunctions induce large interface charges of opposite polarities, which can result in a strong internal electric field and reduced carrier recombination efficiency. As a result, emission from the nonpolar facets can have a much larger gain coefficient than the polar or semipolar facets. Supporting Information Figures S3 and S4 show that the manifestations of the quantum-confined Stark effect, observed

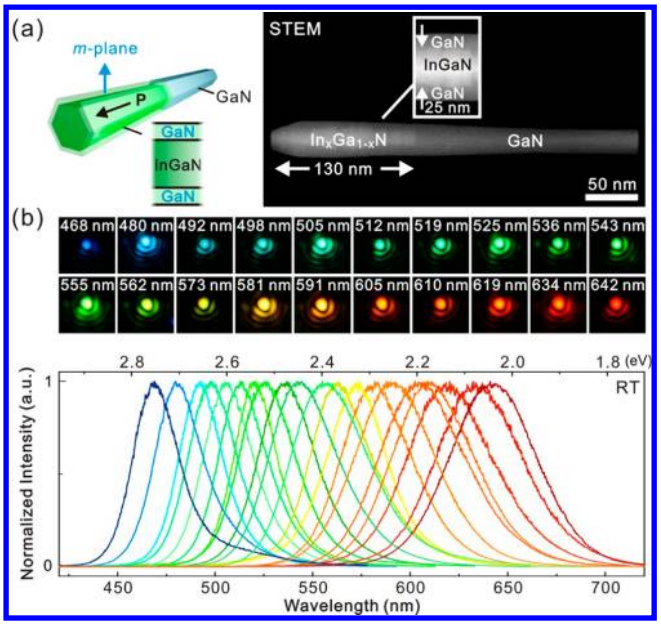


**Figure 1.** $In_xGa_{1-x}N$@ GaN core−shell nanorods exhibiting efficient photoluminescence across the visible spectrum. (a) Schematic of the InGaN@ GaN core−shell nanorod with six nonpolar (*m*-plane) side facets, where P denotes the spontaneous or piezoelectric polarization. The PL emissions from $In_xGa_{1-x}N$@GaN (*x*: In composition) core−shell nanorods remain highly efficient in the long-wavelength (large *x*) region due to the absence of adverse polarization effects in the polar nitride semiconductor heterostructures. The scanning transmission electron microscopy (STEM) image clearly reveals the InGaN@GaN core−shell nanorod structure. The brighter area in this high-angle annular dark-field (HAADF) STEM image indicates the presence of InGaN core due to the atomic mass contrast. The indium composition of InGaN core is ∼9% for the specific nanorod shown here. (b) All-color PL images of the diffraction-limited light emissions from single InGaN@ GaN core−shell nanorods placed on silicon substrates. These images were acquired at room temperature (RT). Emission colors can be tuned from blue (468 nm) to red (642 nm) by different In contents in the nanorods. The corresponding normalized PL spectra show that the emissions from single nanorods are monochromatic with uniform spectral widths (∼150 meV).

for conventional polar InGaN/GaN heterostructures grown along the wurtzite *c*-axis, are negligible for our case.

In Figure 2, we show the schematic structure of a plasmonic nanolaser and the CW lasing characteristics that were measured at low temperature (7 K). In our earlier demonstration of a green CW plasmonic nanolaser, the nanorods were longer (480 nm), resulting in bimodal lasing.[19] In the present study, two refinements were made. First of all, we used shorter nanorods, which lead to single mode lasing. Second, instead of $SiO_2$, we used an $Al_2O_3$ gap dielectric layer grown by atomic layer deposition (ALD), yielding a high-quality dielectric layer with precisely defined thickness, excellent conformity to the deposited surface, and high uniformity over a large area. With this improved gap dielectric, along with atomic smoothness of the epitaxial Ag film, the SPP scattering loss was further reduced, resulting in much lower lasing thresholds.

The scanning electron microscopy (SEM) image shown as an inset in Figure 2a illustrates the detection of localized laser emissions from single nanorods. The nanorods are dispersed onto an $Al_2O_3$-capped epitaxial Ag film by drop casting diluted suspension solutions of nanorods. All-color lasing is accomplished by multiple drop casting, each with nanorods that


dx.doi.org/10.1021/nl501273u | *Nano Lett.* 2014, 14, 4381−4388

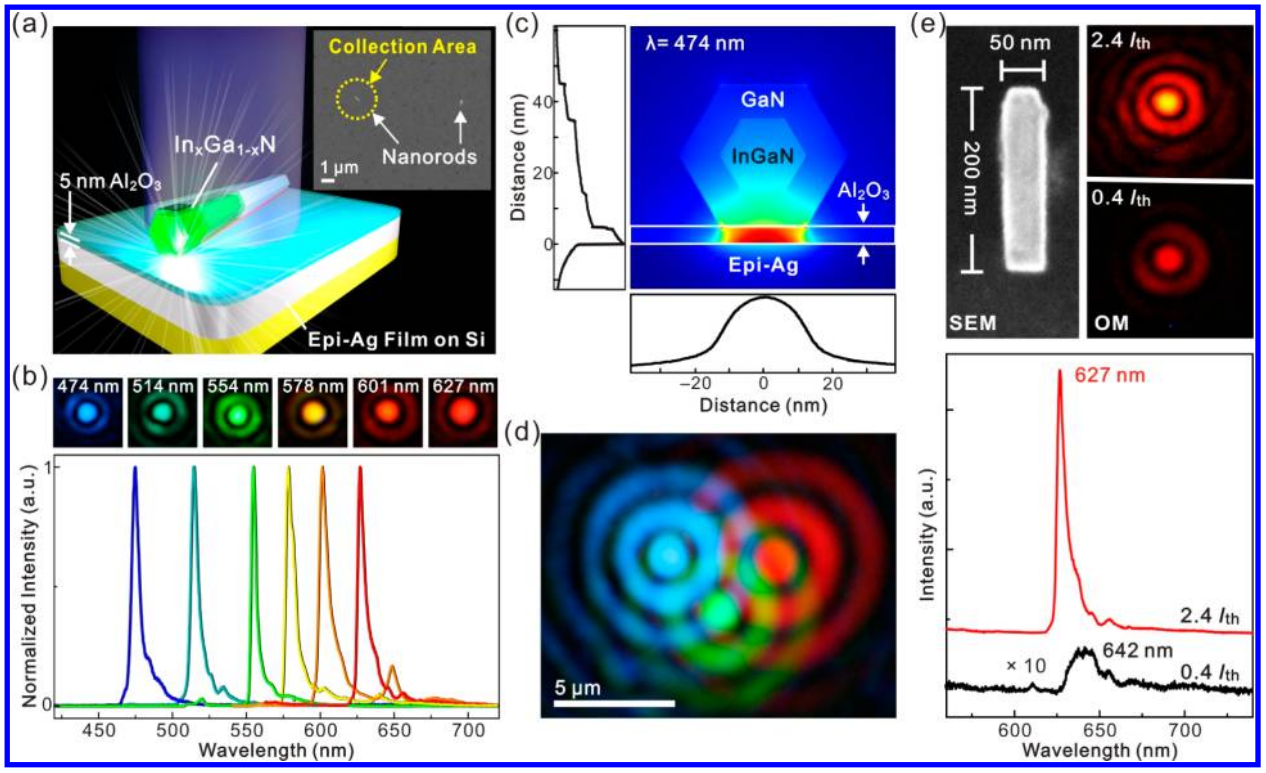


**Figure 2.** All-color InGaN@GaN nanorod plasmonic lasers. (a) Schematic diagram of the nanolaser structure: Single $In_xGa_{1-x}N$@GaN core−shell nanorod were dispersed on the $Al_2O_3$-covered epitaxial Ag film. The scanning electron microscopy (SEM) image on the upper right indicates that we can measure the laser emissions from individual single nanorods with a collection area of about 3 $\mu$m in diameter using a focused excitation laser beam. (b) All-color, single-mode lasing images observed from single nanorods with an emission line width ~4 nm. (c) The simulated energy density distribution of a blue (474 nm) nanolaser. The resonant field is tightly confined in the 5 nm, low-index ($n \approx 1.77$) $Al_2O_3$ gap layer grown by ALD and the plasmonic cavity mode is formed between the nanorod and the epitaxial Ag film. (d) Concurrent RGB lasing from three nanorods placed close to each other. The optical pumping source is a 405 nm, CW semiconductor laser diode with an excitation power density of 3.9 kW/cm$^2$. The scale bar represents 5 $\mu$m. (e) An ultrasmall plasmonic nanolaser emitting at 627 nm (red) that is pumped below (0.4 $I_{th}$) and above (2.4 $I_{th}$) the lasing threshold. Both the OM images and the emission spectra show that a strong frequency pulling effect occurs during transition from spontaneous emission (642 nm) to lasing (627 nm).

contain distinct indium contents within their InGaN cores (see Supporting Information Figure S5). In Figure 2b, we show the broadband tunable radiation of single-mode plasmonic nanolasers in the full visible spectrum. Optical microscopy (OM) images demonstrate single-mode blue, cyan, green, yellow, orange, and red laser emissions from single nanorods, as confirmed by SEM. The optical images observed from single lasing nanorods exhibit clear Airy disk diffraction patterns, also indicating the physical sizes of the emitters are on the subwavelength scale. These single-mode nanolasers have also been confirmed to have highly polarized (nearly 100%) emission along the nanorod axis (Supporting Information Figure S6). Figure 2c shows the calculated energy-density distribution of the nanorod MOS structure by using the 2D eigenmode method for the blue lasing mode (474 nm). The result clearly shows that the electromagnetic field is well confined in the low-permittivity oxide layer with an ultrasmall mode volume. To prepare a sample exhibiting localized all-color emissions (Figure 2d), three diluted suspension solutions of nanorods with different indium contents were sequentially applied to deposit RGB nanorods within close proximity of each other. In Figure 2e, we show the SEM image of a plasmonic nanolaser (~50 nm in diameter, ~200 nm in length) that emits light at 627 nm (red), which is unambiguous evidence for subwavelength lasing. Interestingly, both the OM images and the emission spectra show that a strong frequency pulling effect occurs during the transition from spontaneous emission (642 nm) to lasing (627 nm), which can be well explained by the coupled-mode model.[10,19] Experimentally, we have also confirmed that the pulling of the lasing mode frequency toward the plasmonic resonant frequency strongly depends on the emission wavelength. For example, better spectral matching occurs for the blue nanolaser, resulting in a smaller frequency shift (see Supporting Information Figure S7).

This remarkable demonstration of all-color lasing raises some intriguing questions about the underlying mechanisms involved. In order to achieve multicolor lasing in conventional lasers, such as vertical-cavity surface-emitting lasers, for each individual color, the emitting wavelength of gain medium (colloidal quantum dots)[7] needs to be changed and the cavity length needs to be fabricated individually for spatial and spectral matching with that gain medium.

In the plasmonic nanorod laser (which is actually a spaser because the generating modes are plasmonic[8]), this is no longer necessary. Instead, the all-color lasing reported here is achieved through a novel autotuning mechanism resulting from the interplay between the dispersions of the plasmonic resonator material and the gain medium in a gain-medium-loaded plasmonic nanoresonator. Figure 3a shows the simulated effective index and the corresponding group index ($n_g$, the ratio of the vacuum velocity of light to the group velocity of cavity mode) for a 50 nm width InGaN@GaN core−shell


dx.doi.org/10.1021/nl501273u | Nano Lett. 2014, 14, 4381−4388

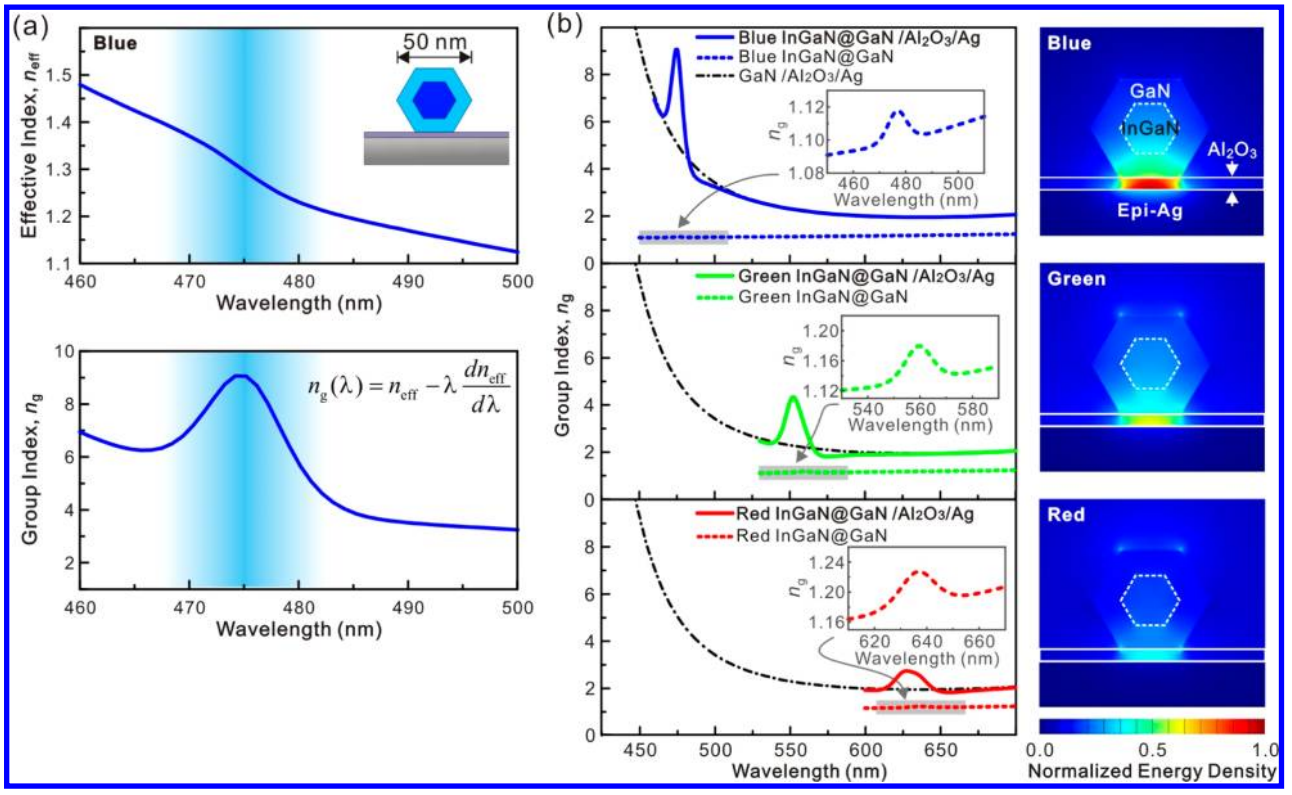


**Figure 3.** Autotuning of plasmonic cavity for RGB single-mode lasing. The simulated MOS structure consists of a 50 nm width, InGaN@GaN core–shell nanorod placed on a 5-nm-$Al_2O_3$ covered, 28-nm-thick epitaxial Ag film. (a) The calculated effective index $n_{eff}(\lambda)$ and the corresponding group index $n_g(\lambda)$ are determined by using the relation $n_g(\lambda) = n_{eff}(\lambda) - \lambda[dn_{eff}(\lambda)/d\lambda]$, where $\lambda$ is the wavelength. The blue-shaded region indicates the emitter line width. The calculation method is described in Supporting Information. (b) The group indices of plasmonic cavity (solid lines) loaded with RGB gain media. In comparison, the insets (dotted lines) show the group indices of bare 50-nm-width InGaN@GaN nanorods (without the epitaxial Ag film) at the PL emission wavelengths of 476, 558, and 637 nm, respectively, whereas the dash-dotted curve depicts the group index of GaN nanorod (without the InGaN core) MOS structure. All the simulation parameters are adopted from the experiment results and known material parameters. Simulations of the energy-density distributions for the RGB plasmonic modes are shown on the right.

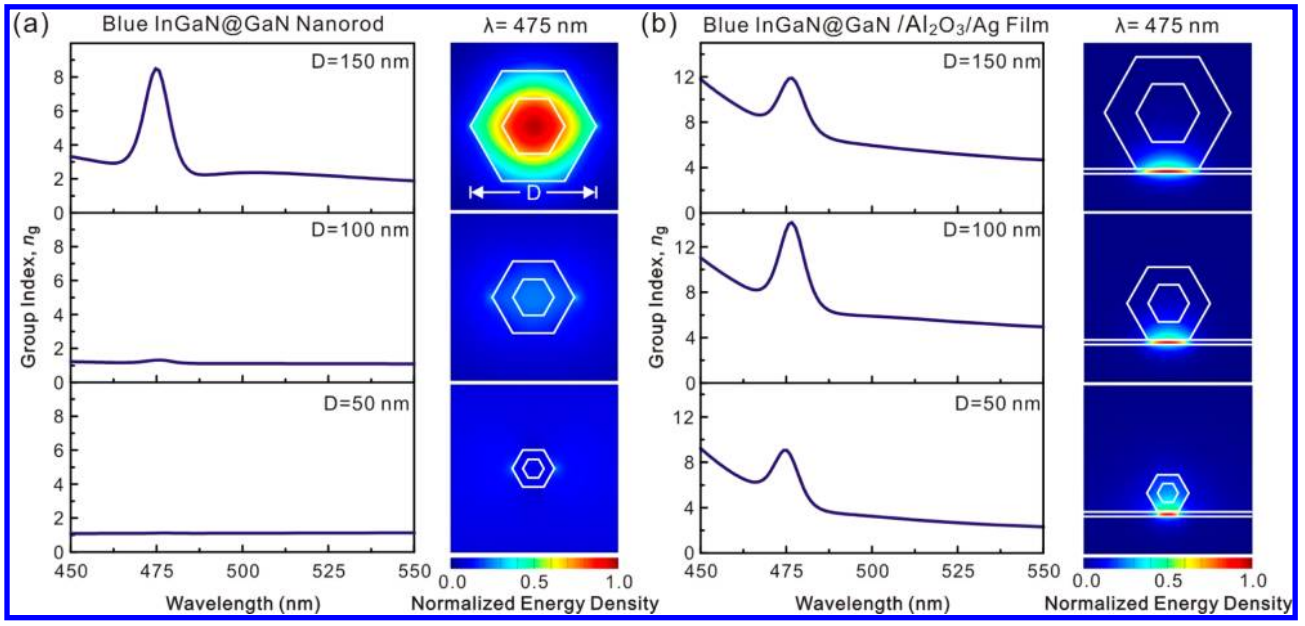


**Figure 4.** Calculated group indices for blue (475 nm) InGaN@GaN core–shell nanorods with varied nanorod diameters. (a) Cases in free space (photonic resonators) and (b) cases supported on an $Al_2O_3$/Ag film (plasmonic resonators). Here, group indices are calculated for blue InGaN@GaN core–shell nanorods with the nanorod diameter varied from 50 to 150 nm. In the presence of a plasmonic cavity, the gain-medium-induced nonlinear enhancement of group index can persist even in the subdiffraction regime.


dx.doi.org/10.1021/nl501273u | *Nano Lett.* 2014, 14, 4381–4388

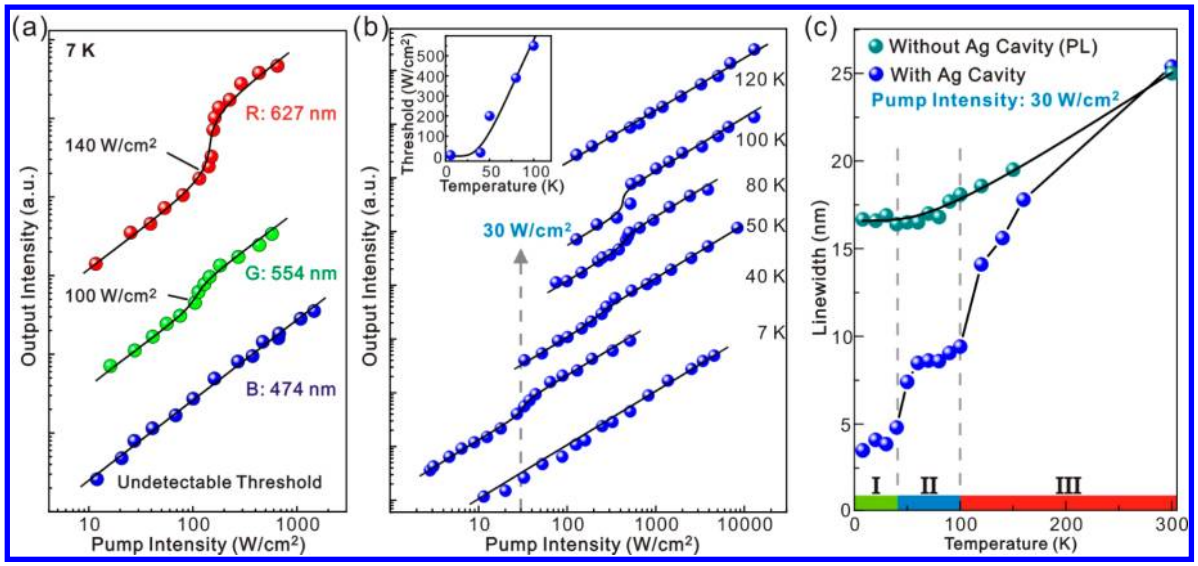


**Figure 5.** Spectral and temperature dependence of lasing threshold and line width. (a) Characteristic $L-L$ plots measured from individual RGB nanolasers. The pumping laser polarization direction was chosen to be perpendicular to the rod axis. Here, plots of the emission peak intensity versus the CW pumping intensity ($L-L$ plots) for blue (474 nm), green (554 nm), and red (627 nm) plasmonic nanolasers are shown for comparison. The different onsets of kinks in the $L-L$ plots indicate that the lasing thresholds are 140 W/cm$^2$, 100 W/cm$^2$, and undetectably small (<10 W/cm$^2$) for red, green, and blue nanolaser, respectively. The fitted spontaneous emission coupling factors ($\beta$) of RGB nanolasers are found to be ~0.3 (red), ~0.7 (green), and ~1.0 (blue) by using a rate equation model. (b) Temperature-dependent $L-L$ plots showing lasing thresholds at temperatures varied from 7 to 120 K for the blue (474 nm) nanolaser shown in panel a, which exhibits an undetectable lasing threshold at 7 K. The inset shows the measured temperature dependence of the lasing threshold. (c) Temperature evolution of the spectral line width for two blue-emitting nanorods measured with and without the plasmonic cavity at varied temperatures from 7 to 300 K. These measurements were performed at a fixed pump intensity of 30 W/cm$^2$, as shown in Figure 5b. The cyan dots represent measurement results for a single InGaN @GaN core−shell nanorod placed directly on a silicon substrate and emitting at 475 nm (RT). The fitted curve exhibits a typical PL line width narrowing behavior. In contrast, the blue dots show the measurement results for the blue (474 nm) nanolaser case with the plasmonic cavity, where we discover a characteristic staircase line width narrowing behavior. Three line width regions can be identified that include the lasing region (I; ~4 nm for $T$ < 40 K), the SPP-coupled PL region (II; ~8 nm for temperature 40 K < $T$ < 100 K) and the gain-medium PL region (III; 100 K < $T$ < 300 K), respectively.

nanorod supported on an epitaxial Ag film with a 5 nm $Al_2O_3$ gap layer (simulation details are described in Supporting Information). The group index is calculated because it can be directly related to the enhanced confinement factor and modal gain in plasmonic resonator.[32,33] In this subwavelength MOS structure, a strong nonlinear enhancement of the group index can be observed at the emission wavelengths of the gain media. In comparison, the insets in Figure 3b show the group indices for free-standing RGB InGaN@GaN nanorods without the Ag film. Because of their subdiffraction size, these group indices are very close to one and exhibit only small peaks at the InGaN emission wavelengths. Also shown, as the black dash-dotted curve, is the group index for the GaN/$Al_2O_3$/Ag hybrid mode in the absence of the gain medium, which exhibits a dispersion curve without the distinct peaks at the InGaN emitting wavelengths. This clearly indicates that this unique feature of "autotuning" results from the interplay between the gain media and the plasmonic cavity material (Ag), which leads to the strong enhancement of group index dispersion around the InGaN emitting wavelengths in the full visible spectrum. Furthermore, the cavity coupling strength shows a strong spectral dependence on the gain-medium emitting wavelength (Figure 3b). For the blue mode, the strong spatial confinement of the electromagnetic field plays an important role to achieve an ultralow lasing threshold.

Figure 4 shows that the group index is size dependent for both photonic and plasmonic resonators. The major difference between these two types of resonators is the field confinement in the subdiffraction regime. Figure 4a reveals for the free-standing cases without the Ag film (photonic resonators) that the group index is very close to unity due to the weak optical field confinement within the nanorod. On the other hand, for the case of a plasmonic resonator (Figure 4b) the gain-medium-induced nonlinear enhancement of group index can persist even in the subdiffraction regime. In fact, the ability to confine the resonant field in the subwavelength-sized dielectric gap region (i.e., $Al_2O_3$ for the present work) is the key novelty of plasmonic nanolasers. For the case of a 50-nm-width InGaN@GaN nanorod supported on an $Al_2O_3$/Ag film (plasmonic resonator), we have confirmed that the group index can still be much larger than unity. In the autotuning mechanism of single-mode lasing, the large enhancement of group index dispersion around the emission wavelength of gain medium can lead to a resonator-length-insensitive lasing mode by adaptively matching an appropriate $n_g(\lambda)$ at the lasing wavelength. Therefore, the broadband nature of enhanced group index enables a wide autotuning bandwidth for individual colors, allowing for simultaneous full-color lasing on the same resonator platform.

In the lasing measurement, the lasing threshold condition is reached when the optical gain in the cavity is sufficient to compensate for the losses, including ohmic loss, far-field radiation into vacuum, and radiation leakage into the substrate. In general, these losses are dependent on the specific cavity mode and the imaginary part of the dielectric function (permittivity) of silver. Recently, it has been theoretically predicted that the cavity loss is a function of the resonance frequency,[11] and the threshold gain of a silver-based plasmonic nanolaser should be on the order $10^3$ cm$^{-1}$. To compare quantitatively lasing thresholds from individual nanolasers, the dependence of an anisotropic absorption coefficient relative to


dx.doi.org/10.1021/nl501273u | Nano Lett. 2014, 14, 4381−4388

the nanorod orientation represents an important factor. Because the nanorod diameter is quite uniform while the length distribution is relatively broad (see Supporting Information for details), the pumping laser polarization was chosen to be perpendicular to the individual nanorod axes in all measurements in the light−light ($L$−$L$) plots shown in Figure 5a. Characteristic spectral dependence of $L$−$L$ curves measured for individual RGB plasmonic nanolasers confirm the coupling mode picture between the gain medium emission and the longitudinal cavity SPP mode.[19] The lasing thresholds of all color nanolasers are ultrasmall (green and red nanolasers, ~100 W/cm$^2$, and even lower for the blue nanolaser <10 W/cm$^2$). This is a significant reduction (more than an order magnitude) in lasing threshold in comparison with our previous report of green nanolaser (~2 kW/cm$^2$) using a similar structure (InGaN/GaN nanorod gain medium on epitaxial Ag platform) but with $SiO_2$ as the dielectric spacer.[19] We believe that this is due to having a better dielectric spacer, provided by the conformal ALD-grown $Al_2O_3$ layer, which further reduces scattering loss. By using a rate equation model (see Supporting Information for details, Supporting Information Figure S8), we found that the fitted spontaneous-emission coupling factor ($\beta$) values for the red nanolaser and green nanolasers are 0.3 and 0.7, respectively, where a larger $\beta$ value indicates a better spectral match. For the blue nanolaser, the apparent $\beta$ value is close to one, resulting from a good spectral match and strong coupling between the gain medium and the resonator SPP mode. Simulation results shown in Figure 3b are also consistent with the spectral dependence of the measured spontaneous-emission coupling factor ($\beta$) of RGB nanolasers.

In Figure 5b, we show the temperature-dependent $L$−$L$ plots for the same blue nanolaser displayed in Figure 5a. At 7 K, a threshold cannot be observed even at a very low excitation power density of 10 W/cm$^2$, implying an upper bound for the threshold. At higher temperatures (between 40 and 100 K), typical "S"-shaped lasing curves appear and the temperature dependence of the lasing threshold can be determined (shown in the inset). At 100 K, the threshold remains relatively low at 550 W/cm$^2$. Interestingly, upon a slight temperature increase to 120 K, we can no longer observe lasing characteristics (see Supporting Information Figure S9 for the line width plots as a function of pump intensity). We attribute this to a strong temperature dependence of nonradiative carrier recombination in gain medium. As shown in Supporting Information Figure S10, the dramatic temperature dependence of the threshold concurs with the onset of significant weakening and line width broadening of the gain medium PL above the same temperature.

In Figure 5c, we show temperature dependence of the line width of the same blue nanolaser shown in Figure 5a at a fixed pump power density of 30 W/cm$^2$, which corresponds to a lasing threshold of this device at 40 K. Through a temperature scan, we reveal three distinct operation regimes. At temperatures below 40 K (labeled as regime I), the emission spectra have the sharpest line (smallest line width), corresponding to the lasing regime. As the temperature is raised, there is a clear and distinct transition above 40 K to an intermediate regime (labeled as regime II), where the line width is roughly twice that of the lasing line width. In this regime, the emission is dominated by the SPP-coupled gain medium luminescence. After the temperature is raised to above 100 K, another transition occurs where the line width quickly increases as a function of the temperate and eventually reaches that of spontaneous emission from the gain medium. In the spaser theory, neglecting the detuning for the blue nanolaser, the spasing (or lasing, if observed in the far-field) threshold is proportional to the square of dipole moment and inversely proportional to emission line width.[10] Therefore, the lasing temperature in the present case is limited by the gain medium, as stated earlier, and is not an intrinsic limitation of plasmonic nanolasers. The observation here qualitatively agrees with the theoretical modeling for the spectroscopic features in these three distinct regimes.[10] Other detailed spectroscopic data and their comparison with the theoretical model are discussed in Supporting Information Figures S11−S13.

The "thresholdless" operation at 7 K for the blue plasmonic nanolaser is strongly suggested by the $\beta$ = 1 fitting of the $L$−$L$ curve shown in Figure 5a,b, and the sharp spectral lines throughout all pump power shown in Figure 6a. More conclusive evidence is provided by the demonstration of temporal coherence by using photon−photon correlation, $g^{(2)}(\tau)$, measurements (see experimental details in Supporting

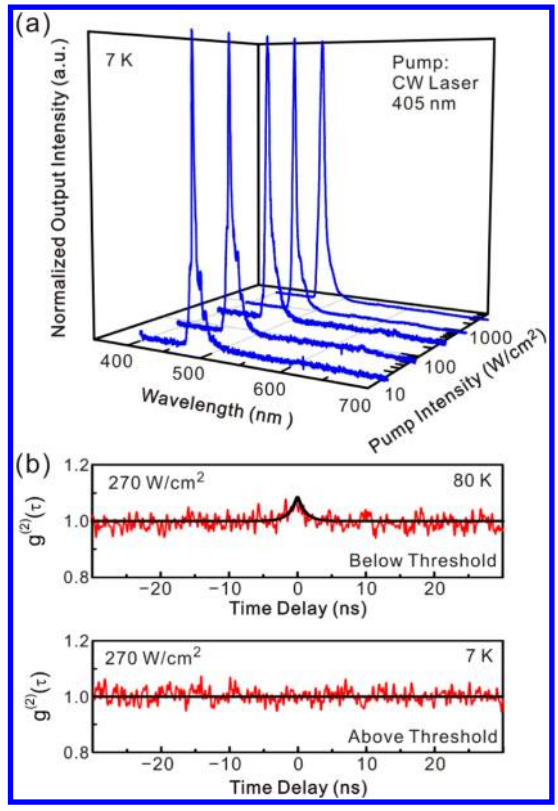


**Figure 6.** "Thresholdless" blue nanolaser. (a) Spectral evolution of emission from the blue plasmonic nanolaser (the same one as shown in Figure 5a) under varying pump intensities ranging from 10 to 1000 W/cm$^2$. The emission maintains a constant lasing line width (4 nm) when measured at 7 K, indicating a "thresholdless" lasing behavior (or alternatively, an undetectable lasing threshold, <10 W/cm$^2$). (b) To confirm the lasing behavior in the time domain, second-order photon correlation functions were measured under the same pump intensity (270 W/cm$^2$) at 80 and 7 K, respectively. As shown in Figure 5b, the pump intensity is right below the lasing threshold at 80 K. Indeed, $g^{(2)}(0)$ is measured to be greater than one, as expected for the case of thermal emission. In comparison, when the pump intensity is above the lasing threshold at 7 K and we confirm that $g^{(2)}(0) = 1$ and remains at unity for all $\tau$, which is an unambiguous signature for the temporal coherence of nanolasing (spasing), it is due to a rapid recovery of plasmon population after emission of a quantum.


dx.doi.org/10.1021/nl501273u | Nano Lett. 2014, 14, 4381−4388

Information Figure S14). Typically, this is accomplished by measuring $g^{(2)}(\tau)$ as a function of the pump power through the threshold and observe the transition of $g^{(2)}(\tau)$ from spontaneous emission to lasing as we have shown previously.[19] Here, we take an alternative approach by measuring $g^{(2)}(\tau)$ at a fixed pump power density by tuning the device across the lasing threshold as a function of temperature. This is necessary since at 7 K the device remains in the lasing regime even at the lowest power density used. Shown in Figure 6b is the $g^{(2)}(\tau)$ measured under a fixed pump intensity (270 W/cm$^2$) at 80 and 7 K, respectively. As expected, $g^{(2)}(0) > 1$ for $T = 80$ K as the pump power is below lasing threshold at this temperature (see Figure 5b). On the contrary, at 7 K we confirm that $g^{(2)}(0) = 1$ and remains at unity for all $\tau$, which is an unambiguous signature for the temporal coherence of lasing (spasing) where the number of surface plasmon quanta recovers rapidly due to the quantum gain after emission of a photon.

It should be noted that the lasing line width is much broader than that predicted by the classical Schawlow–Townes theory. This is due to the ultrasmall size of plasmonic cavities (as the line width is inversely proportional to the population of cavity plasmons)[10] and additional broadening by the semiconductor gain-medium noise.[34] At this pump power density and temperature (80 K), this device is operated in the SPP-enhanced spontaneous emission regime (regime II in Figure 5c) and the line width is still relatively sharp (within a factor of 2 of that in the lasing regime). But the $g^{(2)}(\tau)$ measurement reveals the presence of photon bunching, which is characteristic of the spontaneous emission of the gain medium. This implies that line width alone is not be a conclusive indication of lasing.

In summary, we have achieved gain-composition-tunable, single-mode plasmonic lasing (spasing) in the entire visible spectrum. The most unique feature is that single-mode lasing (spasing) can be reached with subwavelength resonator where the emission wavelength is insensitive to the resonator size. In addition, by optimizing the composing materials in the MOS ($Ag/Al_2O_3/InGaN$) structure, lasing with ultralow thresholds or without appreciable threshold can be achieved due to an almost perfect spectral overlap between the gain medium and the plasmonic mode. These results represent a significant step in the pursuit of ultimate nanolasers and open up a route to a wide range of potential applications in ultrafast information processing, nanoscopy, nanolithography, biomedicine, and ultrasensing.

## ■ ASSOCIATED CONTENT

### Supporting Information

Materials and methods, device fabrication, optical measurements, simulations of gain-medium-loaded nanorod plasmonic cavities, $L-L$ curve fitting using a rate equation model, and additional information, figures, and references. This material is available free of charge via the Internet at http://pubs.acs.org.

## ■ AUTHOR INFORMATION

### Corresponding Authors

*E-mail: gwo@phys.nthu.edu.tw (S.G.).
*E-mail: shih@physics.utexas.edu (C.K.S.).

### Notes

The authors declare no competing financial interest.

## ■ ACKNOWLEDGMENTS

We acknowledge financial support from the Ministry of Science and Technology (MOST) in Taiwan [MOST 102-2628-M-007-001 (S.G.), MOST 102-2221-E-007-145 (L.J.C.), MOST 102-2633-M-007-002 (S.G. and L.J.C), and MOST 102-2633-B-007-001 (S.G.)], the National Science Foundation in U.S.A. [DMR-1306878 (C.K.S.)], and the Welch Foundation [F1672 (C.K.S.)]. For the work of M.I.S., major funding was provided by Grant MURI No. N00014-13-1-0649 from the U.S. Office of Naval Research. Supplementary funding came from Grant DE-FG02-11ER46789 from the Materials Sciences and Engineering Division of the Office of the Basic Energy Sciences, Office of Science, U.S. Department of Energy, Grant DE-FG02-01ER15213 from the Chemical Sciences, Biosciences and Geosciences Division, U.S. Department of Energy, and Grant ECCS-1308473 from NSF. During the Sabbaticals at Munich by M.I.S., his work was supported by the Max Planck Society and the Deutsche Forschungsgemeinschaft Cluster of Excellence: Munich Center for Advanced Photonics (http://www.munich-photonics.de).

## ■ REFERENCES

(1) Yokohama, H. *Science* **1992**, *256*, 66–70.
(2) Noda, S. *Science* **2006**, *314*, 260–261.
(3) Altug, H.; Englund, D.; Vučković, J. *Nat. Phys.* **2006**, *2*, 484–488.
(4) Strauf, S.; Jahnke, F. *Laser Photonics Rev.* **2011**, *5*, 607–633.
(5) Huang, M. H.; Mao, S.; Feick, H.; Yan, H.; Wu, Y.; Kind, H.; Weber, E.; Russo, R.; Yang, P. *Science* **2001**, *292*, 1897–1899.
(6) Schneider, C.; Rahimi-Iman, A.; Kim, N. Y.; Fischer, J.; Savenko, I. G.; Amthor, M.; Lermer, M.; Wolf, A.; Worschech, L.; Kulakovskii, V. D.; Shelykh, I. A.; Kamp, M.; Reitzenstein, S.; Forchel, A.; Yamamoto, Y.; Höfling, S. *Nature* **2013**, *497*, 348–352.
(7) Dang, C.; Lee, J.; Breen, C.; Steckel, J. S.; Coe-Sullivan, S.; Nurmikko, A. *Nat. Nanotechnol.* **2012**, *7*, 335–339.
(8) Bergman, D. J.; Stockman, M. I. *Phys. Rev. Lett.* **2003**, *90*, 027402.
(9) Stockman, M. I. *Nat. Photonics* **2008**, *2*, 327–329.
(10) Stockman, M. I. *J. Opt.* **2010**, *12*, 024004.
(11) Li, D.; Stockman, M. I. *Phys. Rev. Lett.* **2013**, *110*, 106803.
(12) Zheludev, N. I.; Prosvirnin, S. L.; Papasimakis, N.; Fedotov, V. A. *Nat. Photonics* **2008**, *2*, 351–354.
(13) Hill, M. T.; Oei, Y.-S.; Smalbrugge, B.; Zhu, Y.; de Vries, T.; van Veldhoven, P. J.; van Otten, F. W. M.; Eijkemans, T. J.; Turkiewicz, J. P.; de Waardt, H.; Geluk, E. J.; Kwon, S.-H.; Lee, Y.-H.; Notzel, R.; Smit, M. K. *Nat. Photonics* **2007**, *1*, 589–594.
(14) Noginov, M. A.; Zhu, G.; Belgrave, A. M.; Bakker, R.; Shalaev, V. M.; Narimanov, E. E.; Stout, S.; Herz, E.; Suteewong, T.; Wiesner, U. *Nature* **2009**, *460*, 1110–1112.
(15) Oulton, R. F.; Sorger, V. J.; Zentgraf, T.; Ma, R.-M.; Gladden, C.; Dai, L.; Bartal, G.; Zhang, X. *Nature* **2009**, *461*, 629–632.
(16) Ma, R.-M.; Oulton, R. F.; Sorger, V. J.; Bartal, G.; Zhang, X. *Nat. Mater.* **2011**, *10*, 110–113.
(17) Wu, C.-Y.; Kuo, C.-T.; Wang, C.-Y.; He, C.-L.; Lin, M.-H.; Ahn, H.; Gwo, S. *Nano Lett.* **2011**, *11*, 4256–4260.
(18) Khajavikhan, M.; Simic, A.; Katz, M.; Lee, J. H.; Slutsky, B.; Mizrahi, A.; Lomakin, V.; Fainman, Y. *Nature* **2012**, *482*, 204–207.
(19) Lu, Y.-J.; Kim, J.; Chen, H.-Y.; Wu, C.; Dabidian, N.; Sanders, C. E.; Wang, C.-Y.; Lu, M.-Y.; Li, B.-H.; Qiu, X.; Chang, W.-H.; Chen, L.-J.; Shvets, G.; Shih, C.-K.; Gwo, S. *Science* **2012**, *337*, 450–453.
(20) Zhou, W.; Dridi, M.; Suh, J. Y.; Kim, C. H.; Co, D. T.; Wasielewski, M. R.; Schatz, G. C.; Odom, T. W. *Nat. Nanotechnol.* **2013**, *8*, 506–511.
(21) van Beijnum, F.; van Veldhoven, P. J.; Geluk, E. J.; de Dood, M. J. A.; 't Hooft, G. W.; van Exter, M. P. *Phys. Rev. Lett.* **2013**, *110*, 206802.

(22) Müller, J.; Scheubeck, M.; Sabathil, M.; Brüderl, G.; Dini, D.; Tautz, S.; Lermer, T.; Breidenassel, A.; Lutgen, S. *Appl. Phys. Lett.* **2010**, *96*, 131105.
(23) Gather, M. C.; Meerholz, K.; Danz, N.; Leosson, K. *Nat. Photonics* **2010**, *4*, 457−461.
(24) Berini, P.; De Leon, I. *Nat. Photonics* **2012**, *6*, 16−24.
(25) Waltereit, P.; Brandt, O.; Trampert, A.; Grahn, H. T.; Menniger, J.; Ramsteiner, M.; Reiche, M.; Ploog, K. H. *Nature* **2000**, *406*, 865−868.
(26) Nakamura, S.; Pearton, S.; Fasol, G. *The Blue Laser Diode*, 2nd ed.; Springer: Berlin, 2000.
(27) Ohta, H.; DenBaars, S. P.; Nakamura, S. *J. Opt. Soc. Am. B* **2010**, *27*, B45−B49.
(28) Lin, H.-W.; Lu, Y.-J.; Chen, H.-Y.; Lee, H.-M.; Gwo, S. *Appl. Phys. Lett.* **2010**, *97*, 073101.
(29) Lu, Y.-J.; Lin, H.-W.; Chen, H.-Y.; Yang, Y.-C.; Gwo, S. *Appl. Phys. Lett.* **2011**, *98*, 233101.
(30) Ning, C. Z. *Phys. Status Solidi B* **2010**, *247*, 774−788.
(31) Oulton, R. F.; Sorger, V. J.; Genov, D. A.; Pile, D. F. P.; Zhang, X. *Nat. Photonics* **2008**, *2*, 496−500.
(32) Chang, S.-W.; Chung, S. L. *IEEE J. Quantum Electron.* **2009**, *45*, 1014−1023.
(33) Li, D. B.; Ning, C. Z. *Appl. Phys. Lett.* **2010**, *96*, 181109.
(34) Ginzburg, P.; Zayats, A. V. *Opt. Express* **2013**, *21*, 2147−2153.